Magnetic properties and structure of polydisperse ferrofluid models

Tamás Kristóf

Department of Physical Chemistry, University of Veszprém, P.O. Box 158, H-8201 Veszprém, Hungary

István Szalai

Department of Physics, University of Veszprém, P.O. Box 158, H-8201 Veszprém, Hungary

The influence of polydispersity on the equilibrium properties of dipolar systems with short range repulsive interactions (modeled by a shifted and truncated Lennard-Jones pair potential) is studied by means of canonical Monte Carlo simulation and a high field approximation perturbation theory. The particle concentrations and the average magnetic moments of the investigated systems are typical of real ferrofluids. The magnetization curves are calculated and the microstructures are analyzed as a function of density, and the obtained results are compared with the data determined in the monodisperse equivalents of the systems. At weak and moderate magnetic fields the magnetization is found to be generally higher in the polydisperse system than in the corresponding monodisperse one. Our findings for the magnetic properties can partly be explained by the structural characteristics obtained from the simulations.

I. INTRODUCTION

Ferrofluids (ferrocolloids, magnetic fluids) are stable colloidal dispersions of magnetic particles in liquid carriers, which have a wide range of technological applications [1]. The particle size is chosen to be small (4–14 nm) to reduce magnetostatic interactions and the particles are coated with surfactants to prevent aggregation. An important feature of ferrofluids is that each particle in the fluid is a magnetic monodomain, i.e., has a permanent magnetic dipole moment which intensity is fixed, depending on the nature of the material constituting the particles, and proportional to the volume of the particle. Consequently, apart from the usual spherically symmetric interactions: van der Waals attractions and electrostatic or steric repulsions, dipolar particle interactions play a fundamental role in their properties. It can be useful to treat ferrofluids as dipolar fluids, where only the colloidal particles are explicitly taken into account. Many theoretical studies dealing with dipolar fluids take ferrofluids as an experimentally available example of dipolar fluids [2–7].

The physical properties of dilute ferrocolloids can be described adequately in the framework of the one-particle model, which takes ferrocolloid as a gas consisting of noninteracting particles [8]. It is possible to write the equilibrium magnetization by applying the Langevin function, $L(\alpha) = \coth(\alpha) - 1/\alpha$:

$$M_L = \frac{mN}{\mu_0 V} L(\alpha). \qquad (1)$$

Here, m denotes the magnetic moment of a colloidal particle, N is the particle number, V is the volume, $\mu_0 = 4\pi \times 10^{-7}$ H/m, and $\alpha = mH/kT$ represents the Langevin parameter with H being the magnetic field intensity, k the Boltzmann constant, and T the temperature. However, the interparticle interactions play a very important role in concentrated ferrofluids leading to a significant increase

of the initial gradient of the magnetization curve (initial susceptibility) in comparison with the value predicted in Eq. (1) [9].

Real ferrofluids are more or less polydisperse. This means that the nanoparticles are not necessarily the same: they can have different sizes and different magnetic moments. A polydisperse fluid can be considered as a mixture with a large number of components, where the particle size, shape or interaction changes essentially continuously. This additional variable not only affects the equation of state for the system but also the existence of phase transitions. Size polydispersity, for example, has been shown to have a large effect on the coexistence densities. It is known, furthermore, that monodisperse colloidal systems can fill at most ∼60% of space in the liquid state, while colloids with a properly chosen particle-size distribution can be made essentially space filling, both in the solid and in the liquid [10].

The reports on investigation of the influence of polydispersity on the behavior of dipolar systems are scanty in the literature [7,11–14]. From a theoretical point of view a perturbation theoretical study was given by Ivanov *et al.* [11,12] and a cluster expansion study was proposed by Huke and Lücke [13]. The only simulation study using realistic polydisperse models has been carried out in a strongly dipolar hard sphere system where the existence of a spontaneous ferroelectric fluid phase can be observed for the monodisperse case [7]. This work showed that polydispersity either in the magnetic moments or in the size of the hard spheres reduces the ferroelectric order.

In this paper our main concern is the influence of polydispersity on the equilibrium properties of dipolar systems of which particle concentrations and average magnetic moments are typical of real ferrofluids. The magnetization curves are calculated and the microstructures are analyzed as a function of density, and the obtained results are compared with the data determined in the monodisperse equivalents of the systems.

68 041109-1

TABLE I. Experimental data (saturation magnetization M_S, number density N/V) and parameters of the gamma distribution for two ferrofluids [11].

Ferrofluid	M_S (kA/m)	N/V (m^{-3})	$\bar{m}$ (V s m)^a	a	x_0 (nm)	$\bar{x}$ (nm)^b
1	87.1	43.8×10^{22}	2.50×10^{-25}	7.54	0.97	8.2838
2	88.6	42.0×10^{22}	2.65×10^{-25}	2.72	2.03	7.5516

$^a\bar{m}=\mu_0 M_S V/N$.
$^b\bar{x}=x_0(a+1)$.

II. METHOD

A. Models

The systems consist of spherical particles of diameter σ_i, which have permanent point dipole (magnetic) moments m_i. The short range repulsive interaction between particle i and j is modeled by a shifted and truncated Lennard-Jones (sLJ) pair potential [15]

$$\varphi_{ij}^r=4\varepsilon\left[\left(\frac{\sigma_{ij}}{r_{ij}}\right)^{12}-\left(\frac{\sigma_{ij}}{r_{ij}}\right)^6-\left(\frac{\sigma_{ij}}{r_c}\right)^{12}+\left(\frac{\sigma_{ij}}{r_c}\right)^6\right],$$

$$r_{ij}\leqslant r_c=\sigma_{ij}\times2^{1/6}, \quad (2)$$

where ε is the energy parameter, r_{ij} is the interparticle distance, r_c is the cutoff radius, and $\sigma_{ij}=(\sigma_i+\sigma_j)/2$. This cutoff radius ensures that the short range interaction potential is very close to the hard sphere potential. The dipole-dipole potential between particles i and j is given by

$$\varphi_{ij}^d=\frac{1}{4\pi\mu_0}\left[\frac{\mathbf{m_i}\cdot\mathbf{m_j}}{r_{ij}^3}-3\frac{(\mathbf{m_i}\cdot\mathbf{r_{ij}})(\mathbf{m_j}\cdot\mathbf{r_{ij}})}{r_{ij}^5}\right], \quad (3)$$

and the interaction of dipole moments with an external field **H** can be written as

$$\varphi_i^{ext}=-\mathbf{m_i}\cdot\mathbf{H}. \quad (4)$$

To introduce realistic polydispersity into calculations we started from the experimental magnetization curves of two ferrofluids consisting of magnetite particles [11]. The particle polydispersity of these fluids is described by the gamma distribution [16]

$$p(x)=\frac{1}{x_0}\left(\frac{x}{x_0}\right)^a\frac{\exp(-x/x_0)}{\Gamma(a+1)}, \quad (5)$$

where x is the magnetic core diameter of particles, x_0 and a are the parameters of the distribution and Γ denotes the gamma function. Table I shows the parameters of the distribution as well as experimental data for the two ferrofluids. Supposing spherical particles, the mean magnetic moment of the ferrofluid, $\bar{m}$ depends linearly on the bulk magnetization of the ferromagnetic component M_d:

$$\bar{m}=\mu_0 M_d\frac{\pi}{6}\overline{x^3}. \quad (6)$$

Here $M_d=480$ kA/m (solid magnetite) and $\overline{x^3}$ stands for the mean cubed core diameter. To model polydispersity of the

magnetic interactions we assumed that this relation is valid for each individual particle of the ferrofluid, i.e., for particle i, $m_i\propto x_i^3$. In this approach, the polydispersity in size was neglected first, and the particle diameter was chosen to be $\sigma_i=\bar{x}$ (model I). However, the simple equality, $\sigma_i=x_i$, allows us to take into account the size polydispersity of these fluids in a natural way (model II).

B. Theory

In a strong external magnetic field it may be assumed [17,18] that the orientation of magnetic dipole moments is governed mainly by the external field and the dipole-dipole interaction can be considered as a perturbation. According to this assumption the potential energy of this reference system is

$$\Phi_0=\sum_{i<j}\varphi_{ij}^r+\sum_i\varphi_i^{ext}. \quad (7)$$

The reference pair correlation function is given by the product of the pair correlation function of the shifted and truncated Lennard-Jones fluid and the orientation distribution functions of ideal dipoles:

$$g_{ij}(r_{12},\boldsymbol{\omega_1},\boldsymbol{\omega_2})=f_i(\boldsymbol{\omega_1})g_{ij}^{sLJ}(r_{12})f_j(\boldsymbol{\omega_2}), \quad (8)$$

where, e.g.,

$$f_i(\boldsymbol{\omega_1})=\frac{\alpha_i}{\sinh\alpha_i}\exp(\alpha_i\cos\vartheta_1) \quad (9)$$

with $\alpha_i=\mathbf{m_i}\cdot\mathbf{H}/kT$ and ϑ_1 is the angle between the ith dipole and the external field. The corresponding configurational integral is

$$Q_0=Q^{sLJ}\prod_i\frac{\sinh\alpha_i}{\alpha_i}. \quad (10)$$

The long-ranged dipole-dipole interaction [Eq. (3)] is considered as a perturbation and, on the basis of the conventional Mayer function expansion of the configurational integral Q, we obtain

$$\ln\frac{Q}{Q_0}\cong\frac{1}{32\pi^2 V^2}\sum_{i,j}N_iN_j\int d\mathbf{r_1}d\mathbf{r_2}d\boldsymbol{\omega_1}d\boldsymbol{\omega_2}$$

$$\times f_i(\boldsymbol{\omega_1})f_{ij}^M(\mathbf{r_{12}},\boldsymbol{\omega_1},\boldsymbol{\omega_2})g_{ij}^{sLJ}(r_{12})f_j(\boldsymbol{\omega_2}), \quad (11)$$

where

$$f_{ij}^{\mathrm{M}}(\mathbf{r_{12}},\boldsymbol{\omega_1},\boldsymbol{\omega_2})=\exp\left(\frac{\varphi_{ij}^d(\mathbf{r_{12}},\boldsymbol{\omega_1},\boldsymbol{\omega_2})}{kT}\right)-1 \qquad (12)$$

is the dipole-dipole interaction Mayer function. Here, N_i denotes the number of dipoles bearing dipole moment m_i. In the expansion of the configurational integral those terms which contain higher order distribution functions are discarded. To calculate the integrals in Eq. (11) a further approximation is necessary. Here we expand the Mayer functions into first order Taylor series and therefore obtain two types of integrals instead of the original one. The integration with respect to $\boldsymbol{\omega}_1$ and $\boldsymbol{\omega}_2$ can be performed analytically. The remaining integration with respect to $\mathbf{r}_1$ and $\mathbf{r}_2$, using the asymptotic value of the $g_{ij}^{\mathrm{sLJ}}(r_{12})$ pair correlation function, can also be carried out analytically on an infinitely prolate ellipsoid to avoid the depolarization. From the configurational integral [Eq. (11)] the magnetic field dependent free energy can be predicted,

$$F=F^{\mathrm{sLJ}}-kT\sum_i N_i \ln\left(\frac{\sinh \alpha_i}{\alpha_i}\right)$$
$$-\frac{2\pi}{3V}\sum_{i,j} N_i N_j m_i m_j L(\alpha_i)L(\alpha_j). \qquad (13)$$

Assuming continuous polydispersity in dipole moment the free energy can be expressed by the help of integrals containing the distribution function [Eq. (5)].

The derived magnetization function reads

$$M=\frac{N}{\mu_0 V}[\bar{L}(\alpha)+\chi_L \bar{L}(\alpha)\bar{L}'(\alpha)], \qquad (14)$$

where

$$\bar{L}(\alpha)=\int_0^\infty m(\xi)p(\xi)L[\alpha(\xi)]d\xi, \qquad (15)$$

and

$$\bar{L}'(\alpha)=\int_0^\infty m^2(\xi)p(\xi)L'[\alpha(\xi)]d\xi. \qquad (16)$$

In these equations, $L'(x)$ is the derivative of the Langevin function and $\chi_L=m^2 N/3\mu_0 VkT$ is the Langevin susceptibility. It should be noted that in the case of model II the variable ξ is replaced by the molecular diameter variable. It is important to see that the shifted Lennard-Jones reference system does not give any contributions to the magnetic properties in this first order approximation. Furthermore, it is not surprising that the terms of Eq. (14) also appear in a more complicated cluster expansion method proposed by Huke and Lücke [13]. To improve our first order perturbation theoretical approximation the external field strength inside the magnetic fluid is substituted by an effective field strength $\mathbf{H}_e$, which was calculated on the basis of the Weiss model:

$$\mathbf{H}_e=\mathbf{H}+\mathbf{M}/3. \qquad (17)$$

The initial magnetic susceptibility is calculated from the field strength derivative of the magnetization. After some elementary calculation,

$$\chi=\chi_L+\chi_L^2/3 \qquad (18)$$

can be obtained. The aforementioned equation is identical with the first order equation of Ivanov and Kuznetsova [11], and with the formula of Szalai *et al.* [18,19], which was originally derived for the dielectric constant of monodisperse polar fluids.

C. Computational data

Standard canonical Monte Carlo (MC) calculations were performed for the dipolar systems at $T=300$ K using $N=500$ particles. The simulations were started either from a face-centered-cubic lattice configuration with a random distribution of the dipole moment orientations, or from an output configuration of a previous run. The equilibration period in the simulations included 100 000 (monodisperse case) or 500 000 (polydisperse case) cycles, the total length of the production period varied between 400 000 (monodisperse case) and 600 000 (polydisperse case) cycles, and in some cases up to 1 000 000 cycles. Each cycle consisted of N attempted translational and orientational moves of the particles, where the maximum changes were adjusted to obtain a 40–50 % acceptance rate for the move. In the case of the polydisperse systems, each cycle included additional 40–80 cluster moves. A general cluster moving scheme [20] was applied using cluster translation and rotation. Here, for simplicity, all moves leading to an inclusion of a new particle into the cluster were rejected. The clusters were defined on the basis of the pair energies of the interacting particles [21,15]: two particles were considered to be bound if their potential energy was less than 75% of their contact energy in perfect co-alignment.

The long-range dipolar interactions were treated using the Ewald summation with conducting boundary condition [22]. In this case the applied external field is identical to the internal field acting on particles throughout the simulation box.

In the course of the simulations the convergence profiles of the quantities of interest were monitored. Estimates for the error bars were made by dividing the whole runs into 20–50 blocks and calculating the standard deviation of the block averages [23].

The results for the dipolar (magnetic) fluids are presented in reduced units: $T^*=kT/\varepsilon$ is the reduced temperature, $\rho^*=N\sigma^3/V$ is the reduced density, $M^*=M/\sqrt{4\pi\varepsilon/(\mu_0\sigma^3)}$ is the dimensionless magnetization, $H^*=H\sqrt{4\pi\mu_0\sigma^3/\varepsilon}$ is the dimensionless magnetic field, and $m^{*2}=m^2/(4\pi\mu_0\varepsilon\sigma^3)$ is the reduced squared dipole moment, where parameter ε controls the strength of the isotropic repulsion as compared to the dipole-dipole potential. Here we adopted $\varepsilon/k=300$ K and, as we mentioned earlier, $\sigma=\bar{x}$ (note that $\bar{x}$ is different for the two ferrofluids investigated).

The discretization of the particle distribution density $p(x)$ necessary for molecular simulation with limited number of particles is illustrated in Fig. 1. Furthermore, to demonstrate the diversity of the dipole-dipole interaction strength be-
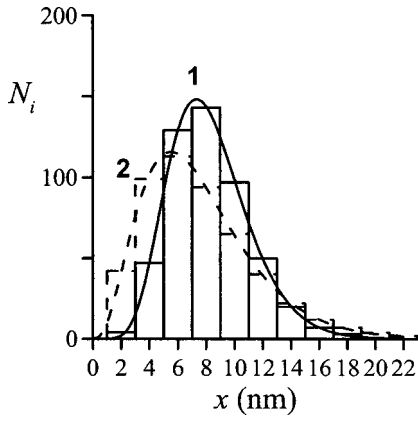
FIG. 1. Discretization of the particle distribution density. Solid and dashed lines represent the Γ distributions for ferrofluids 1 and 2, respectively.

tween two particles of different magnetic core sizes, we tabulated the dipolar coupling constants, $\lambda = m^{*2}/T^*$ at selected particle sizes for ferrofluid 1 (cf. Table II; the magnitudes are the same for ferrofluid 2).

III. RESULTS AND DISCUSSION

Deviations from the Langevin formula [Eq. (1)] clearly reflect the variations in the interparticle interactions, so we begin with the discussion of the magnetization curves. In the simulation the equilibrium magnetization can be obtained from the expression

$$\mathbf{M} = \frac{1}{\mu_0 V} \left\langle \sum_{i=1}^{N} \mathbf{m_i} \right\rangle, \qquad (19)$$

where the brackets denote canonical ensemble average. The calculated magnetization values are displayed in the unit of the saturation magnetization of the ideal ferrocolloid gas,

$$M_S = \frac{\bar{m} N}{\mu_0 V}. \qquad (20)$$

Figure 2 shows the results for the polydisperse ferrofluids 1 and 2 and for their monodisperse equivalents (i.e., $m_i = \bar{m}$ and $\sigma_i = \bar{x}$ for each particle). The magnetization curves from the perturbation theory are given by Eq. (14). According to this expression, the theory does not give any distinction between the two models used. The influence of the density was

TABLE II. Coupling constant λ between two particles of different magnetic core sizes for ferrofluid 1.

Particle 2 \ Particle 1	$x = 4$ nm	$x = 8$ nm	$x = 12$ nm	$x = 16$ nm
$x = 4$ nm	0.01	0.09	0.30	0.72
$x = 8$ nm		0.72	2.42	5.74
$x = 12$ nm			8.17	19.36
$x = 16$ nm				45.88
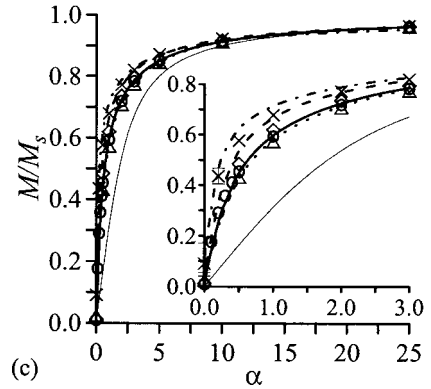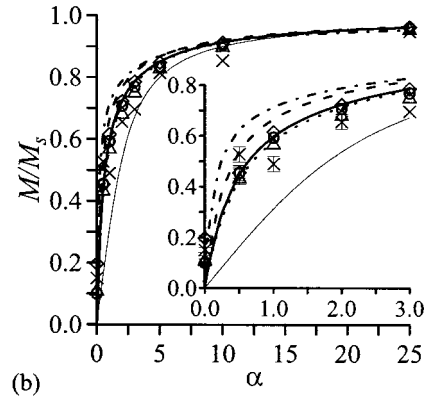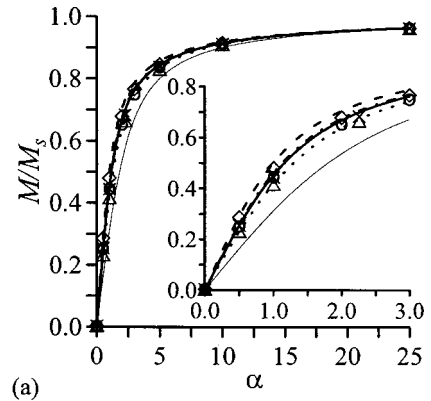
FIG. 2. Dimensionless magnetization as a function of the Langevin parameter for the monodisperse fluids (a), for model I (b), and model II (c). Symbols represent the simulation results and lines are the theoretical predictions. The triangles and the dotted lines correspond to ferrofluid 1 at $\rho^* = 0.1809$, the circles and the solid lines to ferrofluid 1 at $\rho^* = 0.2490$, the diamonds and the dashed lines to ferrofluid 1 at $\rho^* = 0.3500$, and the crosses and the dash-dotted lines to ferrofluid 2 at $\rho^* = 0.1809$. The thin continuous line is drawn to guide the eye: this represents the Langevin function $L(\alpha) = \coth(\alpha) - 1/\alpha$. The statistical uncertainties of the simulation results are only partially displayed in the insets for clarity; error bars are drawn only if the estimated statistical uncertainty is not less than the symbol size. For the polydisperse fluids, $\alpha = \bar{m} H/kT$.

investigated in the case of ferrofluid 1: in addition to the experimental density two different reduced densities, one is just the experimental value for ferrofluid 2, were chosen. The agreement between simulation and theory is "better than qualitative," which verifies the efficiency of this simple first

TABLE III. Initial susceptibility for model II. The numbers in parentheses represent data for the corresponding monodisperse system.

Ferrofluid	$\chi_{\text{simulation}}$	χ_{theory}
1, $\rho^*=0.1809$	7.5±1.5 (1.8±0.7)	5.56 (1.81)
1, $\rho^*=0.2490$	10.5±1.7 (2.7±0.5)	9.05 (2.77)
1, $\rho^*=0.3500$	18.8±2.4 (4.4±0.9)	15.64 (4.49)

order theory. For the monodisperse systems, the theory provides a very good reproduction of the simulation results. The figure also shows that in the polydisperse case the theoretical predictions are weaker. It can be seen that the magnetization curves can be split into two parts. In the range of the strong external magnetic field the differences in magnetization data of the various systems are generally small and becoming progressively smaller with increasing α. The different curves tend to the same limiting value, $M/M_S\approx0.96$; this implies that the high external energy dominates the systems and the magnetization no longer depends on the details of the system's constitution, i.e., the distribution of the particle magnetic moments. At weak and moderate magnetic fields M is generally higher in the polydisperse system than in the cor-

(a)

(b)
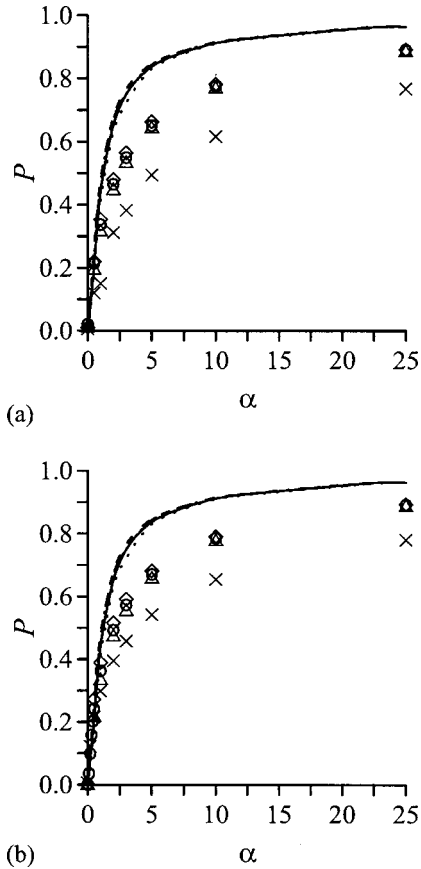
FIG. 3. Order parameter (polarization) as a function of the Langevin parameter for model I (a) and model II (b). The results for the monodisperse fluids are presented as curves fitted to the discrete points for clarity. The meaning of the lines and symbols is the same as in Fig. 2. For the polydisperse fluids, $\alpha=\bar{m}H/kT$.

(a)

(b)
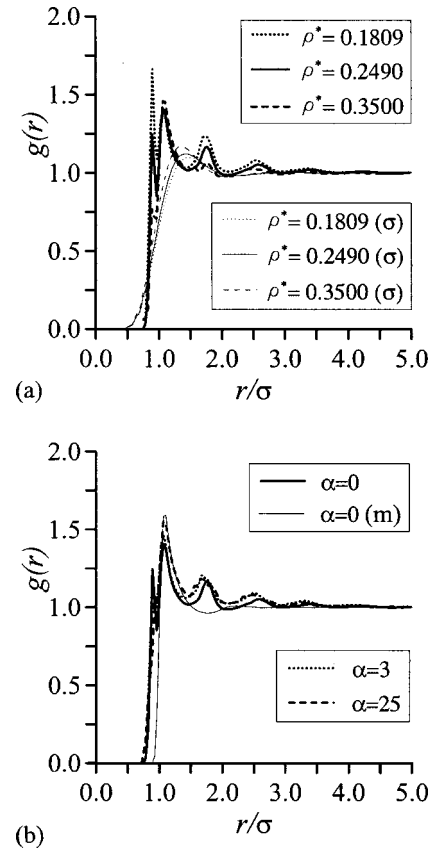
FIG. 4. Pair correlation functions at zero field (a) and at different magnetic fields at $\rho^*=0.2490$ (b) for ferrofluid 1. σ indicates model II and m denotes the monodisperse case.

responding monodisperse system. This difference is more pronounced and evident in the case of model II, while the application of model I has remarkable consequences in the simulation. First, seemingly spontaneous magnetization occurs at zero external field at all the investigated densities for model I. This is due to the formation of large aggregates and we will discuss this point later. Nevertheless, it is obvious that finite size effects are not negligible here. Second, it was necessary to use a cluster-move technique in these fluids because the mobility of the particles with magnetic moments greater than the average magnetic moment is rather low. At a given microstate, there is high probability that such a particle is "cluster-bound" and thus the cluster moves are mostly carried out with the inclusion of particles of larger magnetic moments. However, despite the cluster-move algorithm used, very long simulations are needed even at stronger external fields.

Although the influence of the density on the shape of the magnetization curves seems to be weak, there is a significant density dependence of the initial gradient of the curves. The initial susceptibility, which can be expressed by the linear relationship $\mathbf{M}=\chi\mathbf{H}$ at $H\to0$, was determined from the zero field simulations using the following fluctuation formula [23]:

$$\chi=\frac{1}{3kT\mu_0V}\left(\left\langle\left(\sum_{i=1}^N\mathbf{m_i}\right)^2\right\rangle-\left\langle\sum_{i=1}^N\mathbf{m_i}\right\rangle^2\right).\quad(21)$$

TABLE IV. Average percentage of particles in n-mers at different magnetic fields for model I.

Ferrofluid	α	Dimer	Trimer	(4-8)-mers	(9-39)-mers	(40-)-mers	Σ
1	0	1.2	0.1	0.03	0.2	16.0	17.5
$\rho^*=0.1809$	1	1.5	0.3	0.3	0.6	15.1	17.8
	5	2.5	0.4	0.7	3.9	11.6	19.1
	25	3.5	0.7	1.5	9.9	3.8	19.4
1	0	1.6	0.1	0.1	0.7	15.9	18.4
$\rho^*=0.2490$	1	2.0	0.3	0.4	1.6	14.2	18.5
	5	3.3	0.9	0.6	1.7	13.0	19.5
	25	4.1	0.8	2.1	8.9	4.9	20.8
1	0	2.4	0.2	0.1	0.8	15.3	18.8
$\rho^*=0.3500$	1	2.9	0.5	0.6	2.2	12.9	19.1
	5	4.2	0.9	2.0	9.3	4.0	20.4
	25	5.2	0.9	1.8	12.9	1.5	22.3
2	0	0.8	0.03	0.05	4.4	15.9	21.2
$\rho^*=0.1809$	1	0.9	0.1	0.04	0.2	21.0	22.2
	5	1.5	0.5	0.9	5.4	14.6	23.0
	25	3.0	0.8	1.7	8.8	9.0	23.3

For some monodisperse systems, we have checked the applicability of the formula by comparing our results with literature χ values determined from data of the initial region of the magnetization curves by linear regression fittings [15]. The initial susceptibility data for model II are summarized in Table III. It should be noted that Eq. (21) provides unrealistic results for model I probably because of the large deviations of the calculated magnetization values from zero. The anisotropic behavior cannot be adequately described by the present perturbation theory as well. To estimate the range over which M is directly proportional to α for ferrofluid 1 (in the case of model II and $\rho^*=0.2490$), the magnetization were determined also in the range of α from 0 to 0.5. It can be seen from the enlarged part of Fig. 2(c) that the linear relationship can be considered valid, at most, up to $\alpha=0.2$.

Figure 3 shows the calculated polarization data for the investigated systems. The polarization is defined as the ensemble average of the order parameter P_1,

$$P=\langle P_1\rangle=\frac{1}{N}\left\langle \sum_{i=1}^{N}\frac{\mathbf{m_i}}{m_i}\cdot\mathbf{d}\right\rangle, \qquad (22)$$

where $\mathbf{d}$ is the average (instantaneous) orientation of the dipoles, called the director [21]. Similar to the magnetization curves, the density dependence is also weak here, at least in the moderate and strong field regime. However, the polarization data magnify the existing differences between the systems of various types of polydispersity and between the polydisperse and monodisperse systems. The polarization curves are shifted downward from the curves of the monodisperse systems to those of ferrofluid 2, which means that the ability of the dipoles of these systems to co-align with the field direction reduces with the increase of the proportion of

large dipoles in the systems. Furthermore, it is important to note that P is practically zero for the systems studied in the absence of the external field. The obtained small deviations from zero in the case of polydisperse model I are probably due to finite size effects and do not indicate that these systems exhibit ferroelectric order.

TABLE V. Average percentage of particles in n-mers at different magnetic fields for model II. The numbers in parentheses represent data for the corresponding monodisperse system.

Ferrofluid	α	Dimer	Trimer	(4-8)-mers	Σ
1	0	2.9 (2.9)	0.2 (0.1)	0.01 (−)	3.1 (3.0)
$\rho^*=0.1809$	1	3.0 (3.4)	0.2 (0.1)	0.01 (−)	3.2 (3.5)
	5	3.3 (5.7)	0.2 (0.3)	0.01 (0.02)	3.5 (6.0)
	25	4.2 (7.6)	0.3 (0.5)	0.02 (0.04)	4.5 (8.1)
1	0	4.2 (3.9)	0.4 (0.1)	0.04 (−)	4.6 (4.0)
$\rho^*=0.2490$	1	4.2 (4.6)	0.4 (0.2)	0.04 (−)	4.6 (4.8)
	5	4.7 (7.1)	0.4 (0.5)	0.04 (0.03)	5.1 (7.6)
	25	5.9 (9.2)	0.5 (0.8)	0.05 (0.06)	6.5 (10.1)
1	0	6.2 (5.5)	0.8 (0.3)	0.1 (0.01)	7.1 (5.8)
$\rho^*=0.3500$	1	6.3 (6.3)	0.8 (0.4)	0.2 (0.02)	7.3 (6.7)
	5	6.9 (9.0)	0.9 (0.7)	0.2 (0.06)	8.0 (9.8)
	25	8.5 (11.2)	1.1 (1.1)	0.2 (0.11)	9.8 (12.4)
2	0	4.0 (7.7)	0.3 (0.6)	0.04 (0.04)	4.3 (8.3)
$\rho^*=0.1809$	1	4.0 (8.9)	0.3 (0.8)	0.04 (0.08)	4.3 (9.8)
	5	4.1 (12.9)	0.4 (1.8)	0.04 (0.2)	4.5 (14.9)
	25	4.7 (16.1)	0.4 (2.8)	0.04 (0.5)	5.1 (19.4)

(a)

(b)

(c)
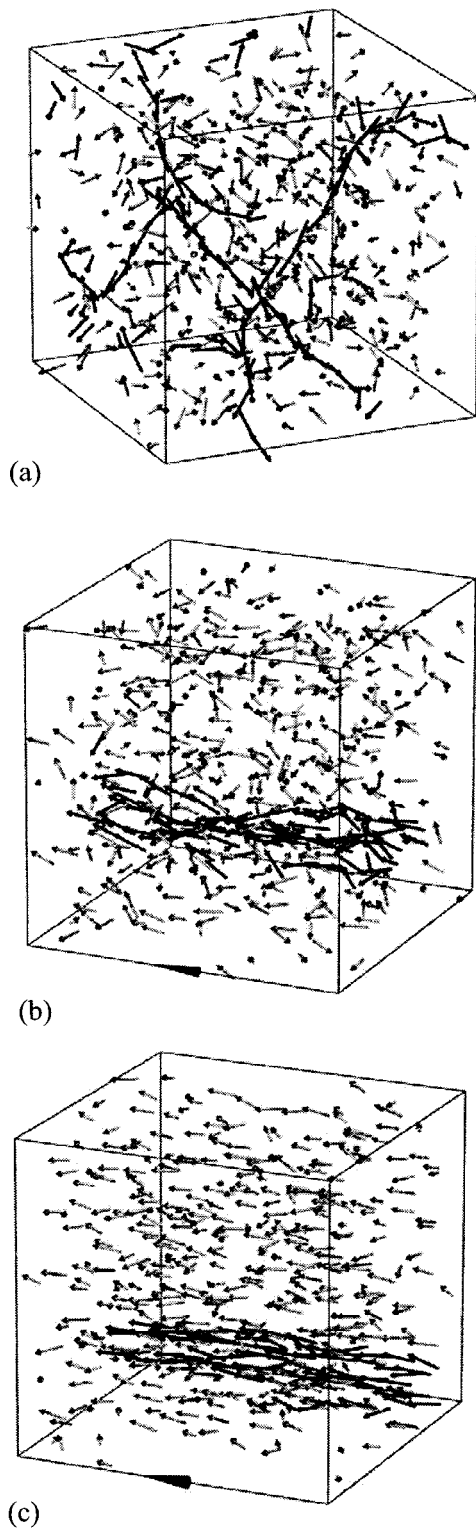
FIG. 5. Snapshots of the simulation cell of ferrofluid 1 at zero field (a), at $\alpha=3$ (b), and at $\alpha=25$ (c) for model I at $\rho^*=0.2490$. The dipolar particles are depicted as arrows with lengths proportional to the magnetic core diameters. Dipoles belonging to the same large cluster are represented in black, the others in gray. The arrow on the frame indicates the direction of the magnetic field.

Figure 4(a) illustrates that there is a marked contrast between the pair correlation functions $g(r)$ produced by using model I and model II for ferrofluid 1 (ferrofluid 2 yields similar results). This is not surprising since the structure in condensed phases is primarily affected by the short range repulsion forces. The comparatively featureless peaks for model II do not reveal association, which resembles, in this respect, the monodisperse case [cf. Fig. 4(b), curve $\alpha=0(m)$]. In contrast, the calculations for the structure of model I demonstrate strong aggregation: a shoulder appears at $r/\sigma<1.0$ and the distances between the peaks are less than 1. The density dependence of the structure is also seen in Fig. 4(a). The height of the peaks slightly increases with the increase of ρ, the only exception being the shoulders in the case of model I. However, noteworthy is that the radial distribution function $J(r)=4\pi r^2\rho g(r)$, which gives the number of particles at a given distance from an arbitrary chosen center, shows approximately the same intensity for these shoulders. When the external field is switched on, the peaks become more intense and the shoulder shrinks. This tendency is represented in Fig. 4(b) at $\rho^*=0.2490$ for model I. The peak height changes similarly also in the case of model II (and for the monodisperse systems), but to a lesser degree, reflecting that the increase of the field strength induces a more ordered state.

The results of our cluster analysis are compiled in Tables IV and V. It is clearly seen that the increase of either the density or the mean magnetic moment of the ferrofluid leads to a larger percentage of particles organized in clusters in the system (see also Table I: $\bar{m}$ is greater for ferrofluid 2 than for ferrofluid 1). The increase of the amount of clusters with the field strength is also an obvious result since the better alignment of the dipoles along the field direction gives a better chance to the particles to form aggregates. Certainly, these clusters are not necessarily stable structures throughout the simulation but are continuously breaking and recombining with other clusters or monomers. In the case of model I, the most striking point is the large proportion of particles found in aggregates. Here, at a given microstate, the majority of particles organized in clusters generally belongs to one large aggregate containing even up to 120 magnetic dipoles. Our analysis showed that nearly all particles with magnetic moments greater than the average magnetic moment can be found in clusters. This is evidently due to the application of a uniform repulsive core size in model I, which enables the particles with larger magnetic moments to get closer to each other. In contrast, the picture is somewhat complicated if we use the magnetic core diameter, x_i for σ_i (cf. Table V). The average percentage of particles in n-mers is mostly smaller than that obtained in the monodisperse system, and it may exceed the corresponding monodisperse value only at zero or weak external fields. The weak field dependence of these data can be attributed to the nonuniform short range repulsive interaction that prevents the close contact of the larger point dipoles. By visual inspection of the three-dimensional configurations formed at different magnetic fields, we have made sure that the structure of the latter polydisperse system

is characterized by randomly distributed short clusters and the resultant dipole moments of these clusters can easily co-align with the field direction.

Finally, let us return to the problem connected with the magnetization curves obtained for model I. At weak and intermediate field strengths large metastability effects were found. Smaller magnetization data were calculated when the simulations were started from a configuration initially equilibrated in the absence of the external field as compared to those obtained in the standard case (a face-centered-cubic lattice configuration with random distribution of the dipole moments). We have to emphasize that the initial configuration dependence can be as large as 40% at $\alpha \lesssim 2$. The snapshot of a typical configuration of the system at zero field [cf. Fig. 5(a)] reveals that a large cluster spreads through the whole simulation box forming a chainlike structure. Here, the nonzero value of M may result from the finite size of the simulated system and indicate this structure rather than a weak ferroelectric phase. Starting from such configurations, the external field can break the previously developed branched chains, within the length of our simulations, only if it is sufficiently strong. In the strong field regime, the system also contains an aggregate with several tens of dipoles, but now this aggregate exhibits a columnlike structure [cf. Figs. 5(b) and 5(c)].

In summary, on the basis of our simulation results we can conclude that the behavior of model II reveals more similarities with monodisperse systems than model I. Under the studied conditions, unlike model II, model I implies the formation of an anisotropic phase. Considering the chain formation, which generally cannot be observed in real ferrofluids in the absence of the external magnetic field, model I is a less realistic polydisperse model, but it may represent an important first step to understand the structure and physical properties of polydisperse dipolar systems. According to the physical picture for magnetic colloids, model II certainly is the better choice for modeling such systems. However, this model does not show any chain formations at strong magnetic fields.

In order to improve the applied theory the inclusion of the higher order perturbation terms would be necessary to obtain better agreement between simulation and theory. Furthermore, to explain the structure of polydisperse systems, either in the absence or in the presence of the external magnetic field, the application of a density functional theory, instead of a conventional perturbation theory, would be worthwhile.

[1] R. E. Rosensweig, *Ferrohydrodynamics* (Cambridge University Press, Cambridge, 1985).

[2] M. E. van Leeuwen and B. Smit, Phys. Rev. Lett. **71**, 3991 (1993).

[3] B. Groh and S. Dietrich, Phys. Rev. Lett. **72**, 2422 (1994).

[4] H. Zhang and M. Widom, Phys. Rev. E **49**, 3591 (1994).

[5] M. J. Stevens and G. S. Grest, Phys. Rev. E **51**, 5976 (1995).

[6] M. A. Osipov, P. I. C. Teixeira, and M. M. Telo da Gama, Phys. Rev. E **54**, 2597 (1996).

[7] B. J. Costa Cabral, J. Chem. Phys. **112**, 4351 (2000).

[8] M. I. Shliomis, Usp. Fiz. Nauk **112**, 427 (1974).

[9] K. I. Morozov and A. V. Lebedev, J. Magn. Magn. Mater. **85**, 51 (1990).

[10] L. Bellier-Castella, H. Xu, and M. Baus, J. Chem. Phys. **113**, 8337 (2000).

[11] A. O. Ivanov and O. B. Kuznetsova, Phys. Rev. E **64**, 041405 (2001).

[12] A. O. Ivanov, Colloid J. USSR **59**, 446 (1997).

[13] B. Huke and M. Lücke, Phys. Rev. E **67**, 051403 (2003).

[14] V. Russier, J. Colloid Interface Sci. **174**, 166 (1995).

[15] Z. Wang, C. Holm, and H. W. Müller, Phys. Rev. E **66**, 021405 (2002).

[16] M. I. Shliomis, A. F. Pshenichnikov, K. I. Morozov, and I. Yu. Shurubor, J. Magn. Magn. Mater. **85**, 40 (1990).

[17] Yu. A. Buyevich and A. O. Ivanov, Physica A **190**, 276 (1992).

[18] I. Szalai, K.-Y. Chan, and Y. W. Tang, Mol. Phys. **101**, 1819 (2003).

[19] I. Szalai, K.-Y. Chan, and D. Henderson, Phys. Rev. E **62**, 8846 (2000).

[20] D. Frenkel and B. Smit, *Understanding Molecular Simulation* (Academic Press, San Diego, 1996), Chap. 12.

[21] D. Levesque and J. J. Weis, Phys. Rev. E **49**, 5131 (1994).

[22] S. W. de Leeuw, J. W. Perram, and E. R. Smith, Proc. R. Soc. London, Ser. A **373**, 27 (1980).

[23] M. P. Allen and D. J. Tildesley, *Computer Simulation of Liquids* (Clarendon Press, Oxford, 1987).